International Journal of Signal Processing, Image Processing and Pattern Recognition
Vol. 8, No. 2 (2015), pp. 41-48
http://dx.doi.org/10.14257/ijsip.2015.8.2.05

Multi-modal Medical Image Fusion Based on Non-subsampled Shearlet Transform

Xing Xiaoxue[1,2], Cao Fucheng[2], Shang Weiwei[2] and Liu Fu[1*]

1.College of Communications Engineering, Jilin University, Changchun 130022, China
2.College of Information Engineering, Changchun University, Changchun 130022, China
E-mail: xiaoxue8184@126.com (Xing Xiaoxue)

**Corresponding author E-mail, liufu@jlu.edu.cn (Liu Fu)*

Abstract

In order to provide more comprehensive and effective information for cancer diagnosis and tumor treatment planning, it is necessary to fuse multi-modal medical images, such as CT/MRI image, CT/PET image, MRI/SPECT image and so on. In this paper, a multi-modal medical image fusion method based on Non-subsampled Shearlet Transform is proposed. Firstly, in this method, source images are decomposed into low-pass and high-pass subbands by NSST. Then, due to the characteristic features--large sparsity and strong contrast, the high-frequency and low-frequency coefficients of the images are fused by the different fusion rules. Finally, the image is reconstructed by the inverse non-sampled shearlet transform. In the method, the fusion rules are designed based on the regional energy and the average gradient; the image entropy, relative quality, average gradient, standard deviation and spatial frequency were used to evaluate the fusion results objectively. In the experiments, CT and MRI images are chosen to verify the method. Both the visual and the objective analysis show that the proposed method is better than the conventional Wavelet-based and non-subsampled Contourlet-based methods.

Keywords: *Multi-modal Medical Images, NSST, Image Fusion, Evaluation Standard*

1. Introduction

With the development of medical technology, medical images play an increasingly important role in medical diagnostics. CT and MRI are both the very important imaging methods. However, based on different medical imaging principles, different medical images can reflect different information about human organs. In addition, more information about lesions location can be read from the images. Various medical images can provide more complementary information. For example, CT images are very clear for bone imaging, and they has relatively low contrast for soft tissue; while, MRI images can better show the soft tissue and the relevant vessel. The goal of multi-modal medical image fusion technology is to put all the multi-source image information together so as to provide a more comprehensive and effective information. Therefore, medical image fusion can solve the problem that the image obtained from a single imaging modality can't provide enough information. At the same time it can provide a more accurate and valuable reference for the medical diagnosis and treatment in [1-4].

Recently, the image fusion algorithms based on multi-scale decomposition have been widely applied in medical image fusion, and the shearlet transform is one of them. For example, in 2011, Li Bin and Wang Lei introduced the non-subsampled shearlet transform (NSST) to the fusion of MRI/SPECT images and CT/PET images in [5].

ISSN: 2005-4254 IJSIP

Shearlet is one of the state-of-the-art MGA tools. From the point of view of approximation theory, the shearlets form a tight frame of well localized waveforms at various scales and directions, which are the true 2-D sparse representation for images with edges. At present, only Curvelet has the similar properties. However, the implementation process of Curvelet is too complex to be achieved within the framework of multi-resolution analysis of the image. Compared with Contourlet and NSCT, the shearlet transformation has the similar implementation process, but it hasn't the restrictions about the number of direction and size of support base. In addition, unlike the NSCT, the inversion of the discrete shearlet transform only requires a summation of the shearing filters rather than inverting a directional filter bank, which suggests that the implementation of the shearlet has more computational efficiency.

However, the shearlet transform is implemented by the sub-sampling scheme, which can bring about pseudo-Gibbs phenomena in the singularities of the images. In this paper, the multi-modal medical image fusion method based on non-subsampled shearlet transform is proposed. In the method, the CT and MRI images are decomposed at different scales and directions by NSST, and the coefficients are fused by various fusion rules. Through the method, the target information can be highlighted; the discontinuities appeared in the image can be eliminated; the effect of fusion is more in line with the human visual requirements.

2. Theory on Shearlet Transform

2.1. The Shearlet Transform

Shearlet transform is made by K.Guo and G.Easley, *et al*., Through using affine system with composite dilations, the shearlet can be reconstructed. It can be used to represent images. At the same time it can be take full advantages of multi-resolution, locality and directionality in [6-8]. In this paper, the medical images are decomposed by shearlet transform to get coefficients of different scales and different directions.

The affine systems are expressed in equation (1) as,

$$A_{AB}(\psi) = \{\psi_{j,l,k}(x) = \left|\det A\right|^{j/2} \psi(B^l A^j x - k) : j,l \in Z, k \in Z^2\} \quad (1)$$

Where, both A and B are 2×2 invertible matrices and $\left|detB\right| = 1$. If forms a parseval tight framework for $L^2(R^2)$, the elements of the system are called composite wavelets.

Shearlets are defined as follows,

$$SH_\psi f(a,s,t) = \left\langle f, \psi_{a,s,t} \right\rangle, a > 0, s \in R, t \in R^2 \quad (2)$$

$\psi_{a,s,t}(x)$ is defined as follows,

$$\psi_{a,s,t}(x) = \left|detM_{as}\right|^{1/2} \psi(M_{as}^{-1}(x-t)) \quad (3)$$

Note that

$$M_{as} = B_s A_a \quad (4)$$

$$A_a = \begin{bmatrix} a & 0 \\ 0 & \sqrt{a} \end{bmatrix} \quad (5)$$

$$B_s = \begin{bmatrix} 1 & s \\ 0 & 1 \end{bmatrix} \quad (6)$$

where A_a is an anisotropic dilation matrix, and B_s is a shear matrix.

As the Formula (2) shows, the shearlet is a set of functions with three parameters which are scale, direction and position. The tiling of the frequency plane induced by shearlet and the frequency support comparision of shearlet and wavelet are illustrated in Figure 1. It can be seen from Figure 1 that the frequency support of shearlet transform is a trapezoidal region which is symmetric relatively for the origin along the direction of the

slope s in different scales. Compared with the wavelet transform, the shearlet can be better to realize the positioning in each of scale, direction and position.

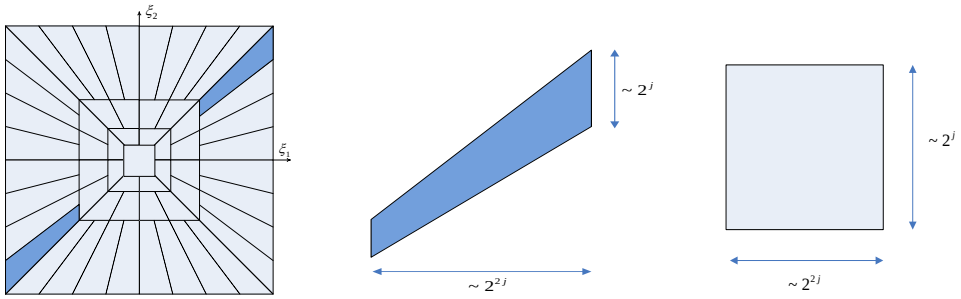

(a) **(b)** **(c)**

Figure 1. The Comparison of Shearlet and Wavelet (a) The Tiling of the Frequency Plane of Shearlet (b) Shearlet Frequency Supports (c) Wavelet Frequency Supports

2.2. Non-subsampled Shearlet Transform--NSST

NSST is comprised of multi-scale partition and directional localization in [9]. In the multi-scale partition, non-subsampled pyramid decomposition is used to reduce the sensitivity to the image shift. In the directional localization, the frequency plane is decomposed into a low-frequency subband and several trapezoidal high-frequency subbands by the non-subsampled shearing filters. The decomposition structure is shown in Figure 2.

In the non-subsampled pyramid filter scheme, in the first level the source image f whose size is $N \times N$ is decomposed into a low-pass image f_a^1 and a high-pass image f_d^1, and in the second level the low-pass image f_a^1 will be decomposed into a low-pass image f_a^2 and a high-pass image f_d^2, and so on. So, if the decomposition level is k , in the end we will get one low-pass image and $k+1$ band-pass images. And the size of all the images is $N \times N$. The directional localization is achieved by the shear filter. In the directional localization scheme, the 2D convolution operation is performed between the band-pass images and the Myer window function. And after that, the subbands images are obtained.

3. Proposed Fusion Algorithm

3.1. Diagram of Fusion Scheme

The medical images have larger sparsity, and the effective detail information of the images can be extracted by NSST. The block diagram of the medical image fusion based on NSST is shown in Figure 3. In Figure 3, LFC represents the low-frequency coefficients; HFC represents the high-frequency coefficients.

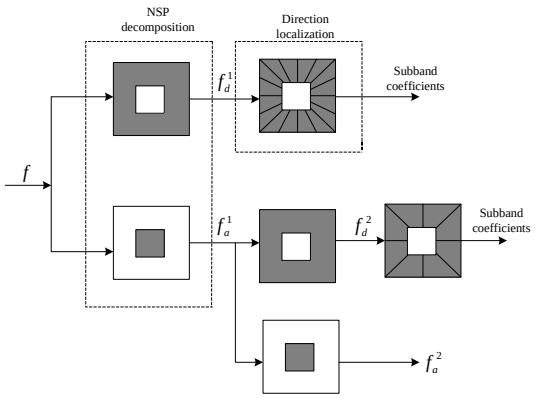

Figure 2. Two Level Decomposition Diagram of NSST

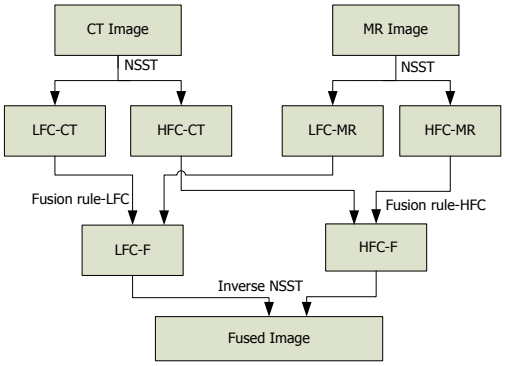

Figure 3. The Diagram of Fusion Scheme

The various implementation steps involved in the proposed fusion algorithm are as follows:

Step1: Decompose the CT image and MR image using Non-subsampled Shearlet Transform into low-frequency components LFC-CT and LFC-MR and high-frequency components HFC-CT and HFC-MR.

Step2: Fuse the LFC-CT and LFC-MR based on the weighted regional energy fusion rule.

Step3: Fuse the HFC-CT and HFC-MR based on the weighted average gradient and energy fusion rule.

Step4: Apply inverse NSST to obtain the fused image.

3.2. The Selection of Fusion Rules

3.2.1. Fusion Rule of Low-frequency Components

The coefficient of low frequency represents contour information, and which is approximation of source images and don't have sparsity. In the paper, the coefficient of low frequency is fused based on weighted regional energy.

Step1: Calculate the regional energy.

The low-pass coefficients of the source images are A_L and B_L, the size of the images is $n \times n$, the regional energy is E_{AL} and E_{BL} respectively, the window function is v.

$$v = \frac{1}{8}\begin{bmatrix} 0 & 1 & 0 \\ 1 & 4 & 1 \\ 0 & 1 & 0 \end{bmatrix} \tag{7}$$

$$E_{pL} = \sum_{k=-n'}^{n'} \sum_{r=-n'}^{n'} f_p^2(i+k, j+r)v(i+k, j+r), p = A, B \tag{8}$$

Where, n is the number of the row, $n' = \left[\frac{n}{2}\right]$, $f_p(i, j)$ means the low-pass coefficients of the pixel (i, j), $v(i, j)$ means the corresponding element of pixel (i, j) in the window function v.

Step2: Calculate the weights.

The weight coefficient ω_{LA} and ω_{LB} are given by:

$$\begin{cases} \omega_{AL} = E_{AL} / (E_{AL} + E_{BL}) \\ \omega_{BL} = E_{BL} / (E_{AL} + E_{BL}) \end{cases} \tag{9}$$

Step3: Calculate the low-pass coefficients of the fused image.

The coefficient of low frequency F_L after fusion is given by:

$$F_L(i, j) = \omega_{AL} * A_L(i, j) + \omega_{BL} * B_L(i, j) \tag{10}$$

3.2.2. Fusion Rule of High-frequency Components

The coefficient of high frequency represents detail information, and which has large sparsity. The coefficient of high frequency is fused based on weighted average gradient and energy.

Step1: Calculate the regional energy.

The high-pass coefficients of the source images are A_H and B_H, the regional energy E_{AH} and E_{BH} are calculated by the formula (7-8).

Step2: Calculate the regional average gradient.

$Grad_{AH}$ and $Grad_{BH}$ are the gradient.

$$Grad_{pH}(i, j) = \frac{1}{n \times n} \sum_{k=-n'}^{n'} \sum_{j=-n'}^{n'} \sqrt{\frac{\Delta F_x^2(i+k, j+r) + \Delta F_y^2(i+k, j+r)}{2}}, p = A, B \tag{11}$$

Where, ΔF_x and ΔF_y are the variance of the image along x axial and y axial.

Step3: Calculate the weights.

The weight coefficient ω_{HA} and ω_{HB} is given by:

$$\begin{cases} \omega_{AH} = Grad_{AH} / (Grad_{AH} + Grad_{BH}) \\ \omega_{BH} = Grad_{BH} / (Grad_{AH} + Grad_{BH}) \end{cases} \tag{12}$$

Step4: Calculate the high-pass coefficients of the fused image.

The coefficient of high frequency F_H after fusion is given by:

$$F_H(i, j) = \begin{cases} A_H(i, j), & E_{AH} > E_{BH} \text{ and } Grad_{AH} > Grad_{BH} \\ B_H(i, j), & E_{AH} < E_{BH} \text{ and } Grad_{AH} < Grad_{BH} \\ \omega_{AH} * A_H(i, j) + \omega_{BH} * B_H(i, j), & \text{else} \end{cases} \tag{13}$$

4. Experimental Results and Discussion

In order to evaluate the effectiveness and the validity of the proposed algorithm, the two sets of medical images are chosen to conduct the experiments. All the images are the same size of 256×256. All the images used can be downloaded from the Harvard university site. The corresponding pixels of the two source images have been perfectly co-aligned before fusion. The source images are shown in Figure 4. The Figure 4 (a) - (b) is the CT and MRI images of normal human head; the Figure 4 (c) - (d) is the CT and MRI images of normal human brain. The experiments are done in the PC with the Intel CPU 3.4 GHz and 8G RAM, operating under Matlab R2011a.

In this paper, in the same fusion rule the Wavelet-based in [10], the NSCT-based in [11-12] and the NSST-based methods are compared. In the WT fusion method, the "Db4" wavelet is chosen as the decomposing wavelet and the decomposition level is set 5. In the NSCT fusion method, the decomposition level is set 2. In the proposed method, the decomposition level is 3, and the number of the directions is 4, 8 and 16. All the fusion results are show in Figure 5 and Figure 6, Table I and Table II respectively.

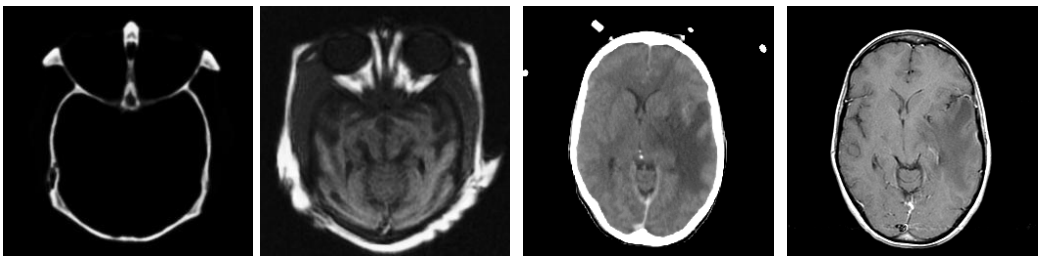

(a) (b) (c) (d)

Figure 4. Source Images (a) CT Image of Normal Human Head (b) MRI Image of Normal Human Head (c) CT Image of Normal Human Brain (d) MRI Image of Normal Human Brain

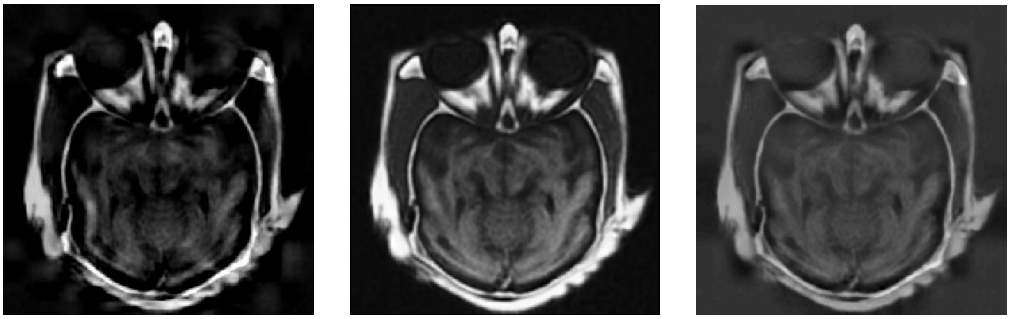

(a) Wavelet fusion (b) NCST fusion (c) Proposed method

Figure 5. Comparison Results of Fusion Methods in First Set Image

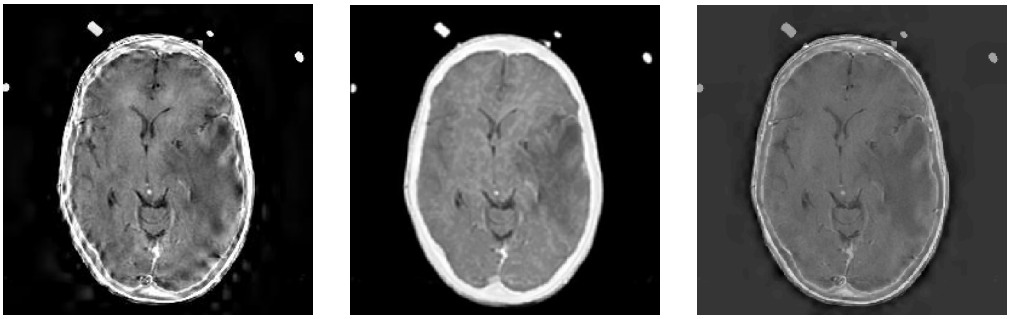

(a) Wavelet fusion (b) NCST fusion (c) Proposed method

Figure 6. Comparison Results of Fusion Methods in Second Set Image

As shown in Figure 5-6, from a subjective point of view the proposed algorithm can get the better fusion results, and the fused image is more clear and accurate. The quality of the fused image could be better.

The image entropy (E), relative quality (Qabf), average gradient (AG), standard deviation (SD) and spatial frequency (SF) were used to evaluate the fusion results objectively. The comparison results of 3 methods are shown in Table I and Table II.

Table I. Performance Evaluation of Various Methods for First Set of Medical Image

	E	AG	SD	Q(abf)	SF
WT Fusion	6.80	6.87	60.48	0.67	16.92
NSCT Fusion	6.84	6.97	61.08	0.77	17.62
NSST Fusion	**7.56**	**7.72**	**56.99**	**0.79**	**19.68**

Table II. Performance Evaluation of Various Methods for Second Set of Medical Image

	Entropy	AvGrad	StD	Q(abf)	SF
WT Fusion	4.27	4.89	80.48	0.28	17.89
NSCT Fusion	4.37	4.88	80.42	0.39	17.17
NSST Fusion	**5.85**	**10.53**	**80.48**	**0.55**	**34.05**

As shown in Table I and Table II, compared with other methods, the fusion results applied the NSST technology is better. The presented algorithm in the paper has higher image entropy. In addition, the contour of the image is more clear and bright.

5. Conclusion

In this paper, a multi-modal medical image fusion method based on non-subsampled shearlet transform is presented. Compared with the traditional multi-resolution image fusion methods, the proposed method can effectively overcome the Gibbs phenomenon, and has more accurate and higher computing efficiency. Compared with the traditional fusion rules, the proposed fusion rules fully consider the characteristics of medical images, which make not only full use of the image contour information, but also reflects the image edge information. Both the visual and objective analysis show that the proposed method is not only can be used in the medical image fusion, but also better than the wavelet and other commonly used multi-scale geometric analysis tools. The presented method has broad application prospects.

Acknowledgements

The authors would like to thank for the developers of the shearlet toolbox, contourlet toolbox and the NSCT toolbox. This work is supported by Jilin Province Education Department (No. 20140529).

References

[1]. M. Freiman, M. Werman and L. Joskowicz, "A curvelet-based patient specific prior for accurate multi-modal brain image rigid registration", Medical Image Analysis, vol. 15, no. 1, **(2011)**, pp. 125-132.
[2]. G. Bhatnagar, Q. M. Wu and L. Zheng, "Human visual system inspired multi-modal medical image fusion framework", Expert Systems with Applications, vol. 40, no.5, **(2013)**, pp. 1708-1720.
[3]. C. T. Kavitha, C. Chellamuthu and R. Rajesh, "Medical image fusion using combined discrete wavelet and ripplet transforms", Procedia Engineering, vol. 38, **(2012)**, pp. 813-820.
[4]. S. Daneshvar and H. Ghassemian, "MRI and PET image fusion bycombining HIS and retina-inspired models", Information Fusion, vol. 11, no. 2, **(2010)**, pp. 114-123.
[5]. L. Wang, B. Li and L. F. Tian, "Multi-modal medical image fusion using the inter-scale and intra-scale dependencies between image shift-invariant shearlet coefficients", vol. 19, **(2014)**, pp. 20-28.
[6]. M. Qiguang, S. Cheng and X. Pengfei, "A novel algorithm of image fusion using shearlets", Optics communications, vol. 284, no. 6, **(2010)**, pp. 1540-1547.
[7]. C. Z. Deng, S. Q. Wang and X. Chen, "Remote sensing images fusion algorithm base on shearlet transform", Proceedings of the 2009 International Conference on Environmental Science and Information Application Technology, **(2009)** July 4-5, Wuhan, P. R. China.

[8]. K. GUO and D. LABATE, "Optimally Sparse Multidimensional Representation using Shearlets", SIAM JMathl Anal, vol. 39, **(2007)**, pp. 298-318.
[9]. G. Easley, D. Labate and W. Lim, "Sparse Directional Image Representation using the Discrete Sheralet Transform", Appl Comput Harmon Anal., vol. 25, no. 1, **(2007)**, pp. 25-46.
[10]. R. Singh, M. Vatsa and A. Noore, "Multimodal medical image fusion using redundant discrete wavelet transform", Proc of 7th Int Conf Advances in Pattern Recognition, **(2009)** Feb. 4-6, Kolkata, India.
[11]. A. L. Cunha, J. Zhou and M. N. Do, "The nonsubsampled contourlet transform: Theory, design, and applications", IEEE Trans on Image Proc., vol. 15, no. 10, **(2006)**, pp. 3089-3101.
[12]. X. X. Xing, F. Liu, W. W. Shang, Y. Lei and J. Shujiao, "Medical Image Fusion In Compressed Sensing Based on Non-sampled Contourlet Transform", 2013 IEEE 9th International Conference on Mobile Ad-hoc and Sensor Networks, **(2013)** December 11-13, Dalian, P. R. China.

